TOPOLOGY OPTIMIZATION FOR 3D MATERIAL DISTRIBUTION AND ORIENTATION IN ADDITIVE MANUFACTURING

D. Jiang and D. E. Smith

Department of Mechanical Engineering, Baylor University, Waco, TX 76712

Abstract

Products produced with Additive Manufacturing (AM) methods often have anisotropic microstructure that forms as material layers are added during processing. Unfortunately, current AM design methods do not accommodate the inherent non-isotropic behavior of these materials when determining the best structural layout. This paper presents a three dimensional (3D) topology optimization method that computes the best non-isotropic material distribution and principal material direction for minimum compliance of a statically loaded non-isotropic AM structure. The compliance objective function is calculated using the finite element method with eight node 3D isoparametric elements, and design sensitivities with respect to both density and material orientation are calculated with the Adjoint Variable method. We employ a linear weighted sensitivity filter on the density variables to mitigate checker-boarding of the material distribution. The optimization problem is solved with a nonlinear constraint-based Matlab (The Mathworks, Inc., Natick, MA) optimization solver. Topology optimization of a 3D cantilever beam with different print directions is given to demonstrate the applicability of the optimization scheme.

Introduction

The Fused Filament Fabrication (FFF) deposition process directs thermoplastic polymer feedstock through a heated nozzle which is then deposited onto a platform as a bead to print a part, layer-by-layer, based on data from a digital model of the part. The mechanical properties of the printed parts depends on the deposited material and the orientation of the printed bead [1–3], where the influence of bead direction is more pronounced when short fiber polymer composites are employed. Carbon fiber filled polymer deposited in beads with the FFF process has been shown to have a highly non-isotropic material response. The non-isotropic topology optimization method presented here is applicable to any AM method that produces oriented microstructure, however, our primary focus is on designing FFF printed parts using carbon fiber filled (CFF) polymer feedstocks.

Fused Filament Fabrication

The FFF process can be categorized into two types. The first is for small scale 3D printing application, which uses a polymer or polymer composite filament as the feedstock. Small scale FFF has a continually growing market [4] and is popular among hobbyist and academic research. There are several drawbacks in small scale FFF. The size of the fabricated parts is limited by build volume which is typically less than one cubic foot. The dominant type of the material for small scale FFF is thermoplastic, which has weaker mechanical properties than metals, limiting the use of FFF parts in industry. Various kinds of composite filaments have been

emerged to improve the filament's mechanical properties [5–12]. In this case short carbon fibers (CFs) are suspended within the polymer matrix to form a carbon fiber filament (CFF). Researchers have shown that CFF polymer filament has improved tensile strength and stiffness as compared to the unfilled polymer [11–13]. It can further reduce the warpage of the structure after the print process [14], due to lower coefficient of thermal expansion and higher thermal conductivity of the CFs as compared to the thermoplastic polymer.

The second category of FFF is large scale 3D printing. It aims to print objects in large size with polymer nozzle exit diameters approaching $^1/_2$ inch. Advances in large scale 3D printing have grown considerably in recent years, where the most prominent example is the Big Area Additive Manufacturing (BAAM) technology. The BAAM system is based on gantry system with build volumes on the order of feet, and discontinuous CFF polymer pellets that is used as feedstock for printing. It requires lower energy input and gives higher material output per unit time than small scale 3D printing [15]. Beside the BAAM system, other institutions have created large 3D printers and print objects with CFF polymer pellets [16]. The adoption of large scale 3D printing is pushing the application envelope of FFF to industrial application, and the demand for lighter and stronger product is expected to drive the polymer composite industry to be more competitive in the 3D printing market. The application of FFF with CFF polymer feedstocks offers unique advantage as the fibers align highly within a bead along the printing direction [12], making it possible to predict the mechanical properties of the parts before it is even printed.

Topology Optimization and Additive Manufacturing

Topology optimization is a simulation tool for computing the optimum layout of a structure within a given design domain to minimize a defined objective, given prescribed design constraints. In structural mechanics, the compliance of the structure commonly serves as the objective to be minimized as this results in the stiffest design. There are numerous topology optimization approaches, including Homogenization Method [17,18], Solid Isotropic Material Method (SIMP) [19–24], Evolutionary Structural Optimization Method (ESO) [25] and Bidirectional Structural Optimization Method (BESO) [26].

Topology optimization has been used for various AM techniques. Zhang, et al. [27] employed the homogenization, optimization and construction (HOC) technique to design variable cellular structures. In their approach, the cellular structure was constructed based on the optimized density distribution using a method similar to SIMP, and the part was fabricated with stereolithography. Gaynor, et al. [28] implemented a combinatory and multiphase SIMP approaches to optimize the shape of compliant mechanisms where the optimized topology may include more than one type of material. Their optimized result was fabricated using the multimaterial Polyjet 3D printing technique. Furthermore, Langelaar [29] proposed a numerical scheme to create a self-support structure for AM purpose.

Simultaneous Topology and Material Orientation Optimization

In this paper, we extend the SIMP method to be applicable to AM structures having non-isotropic materials. The SIMP method assigns an isotropic material model in each discretized finite element, multiplied by a density value raised to an integer power. The exponent serves as a penalization to drive the solution field to a discrete (black and white) layout. The SIMP method

can be modified to accommodate anisotropic materials by including a constitutive material model [30,31] with predefined preferred orientation; this modification is called Solid Orthotropic Material Penalization (SOMP), or the Continuous Fiber Angle Optimization (CFAO) when applied to fiber filled composites in FFF [32,33]. Jia et al. [30] applied the SIMP method with material orientation variables to design fiber reinforced composites for minimum compliance. The optimized topology appears with minor checkerboard effect, as filtering [34,35] that is commonly applied to avoid these unwanted patterns appears to be missing. Setoodeh, et al. [36] developed a stress based SIMP approach to solve for minimum compliance, combined with cellular automata. They further extended the method to solve problems with multiple loads, though the material angle update scheme was based on a random search approach. Nomura, et al. [37] proposed a general topology optimization approach based on discrete angle sets that simultaneously optimizes both material distribution and material orientation. In their approach, orientation variables are represented by Cartesian components, along with relaxation of the orientation design space**.** In other work, Hoglund [38] extended the SIMP method to accommodate material orientation designated as the CFAO. In this approach, design sensitivities with respect to the density and material orientation were derived, and the density sensitivity was also filtered using a linear weight-average filter [34,35]. The optimized model was then printed with desktop 3D printer.

Prior works given above included material distribution and material orientation in two dimensions, and did not include 3D AM structures. To author's knowledge, the literature has yet to address topology and material orientation optimization for the application of FFF printed parts in 3D. This paper proposes a computational scheme that optimizes material distribution and material orientation that is applicable to FFF. Our method extends the SIMP method, similar to the work done by Hoglund [38]. An important assumption to make in 3D design is that since the FFF printed parts are made through a layer-by-layer process, the rotation of the material orientation is constrained in the print plane. This assumption is made since fibers align along the print direction which also reduces the complexity of the design problem. The optimization scheme developed here provides insight into the optimal topology and the bead pattern of the printed part, therefore making the FFF process more efficient and competitive in the market.

Methodology

Optimization Formulation

We consider the topology optimization problem to minimize the compliance of a structure with design constraints which is written as

$$\text{Minimize: } c(\boldsymbol{\rho}, \boldsymbol{\theta}) = \mathbf{U}^{\mathbf{T}}\mathbf{F} = \mathbf{U}^{\mathbf{T}}\mathbf{K}\mathbf{U} = \sum_{e=1}^{N} (\rho_e)^p \mathbf{u}_e^T \mathbf{k}_e(\theta_e)\mathbf{u}_e \tag{1}$$

$$\text{Subject to: } \frac{v(\boldsymbol{\rho})}{V_0} = f, \mathbf{K}\mathbf{U} = \mathbf{F}, \rho_{min} \le \rho_e \le 1, -2\pi \le \theta_e \le 2\pi \tag{2}$$

In the above, *c* is the compliance and **K**, **U** and **F** are the global finite element stiffness matrix, displacement vector and load vector, respectively. The compliance is calculated by summing all

the elemental compliances where $\mathbf{k_e}$ and $\mathbf{u_e}$ respectively represent the stiffness matrix and displacement vector at the elemental level. The material volume $v(\rho)$ is limited by that of the design domain V_0 with the prescribed volume fraction f which ranges from 0 to 1. There are in total N elements in the design domain, and each element is assigned one ρ_e and one θ_e. A penalization parameter p is included which tends to drive the each density variable ρ_e to its lower or upper limit. The material orientation variable θ_e has a lower and upper limits of -2π and 2π, respectively. Again, material orientation is assumed to only vary within the print plane, requiring only one orientation variable for each element. The finite element method is used to evaluate compliance such that static equilibrium is enforced.

Isoparametric Hexagonal Element

The CFAO approach defined in Equations (1) and (2) extends the SIMP method through the addition of the element material orientation design variables θ_e. Therefore, the element stiffness matrix $\mathbf{k_e}$ that is constant for a uniform mesh in the SIMP method varies over the design domain in CFAO. In our implementation, the elemental stiffness matrix is evaluated using the eight-node isoparametric hexahedral element [39] appearing in Figure 1.

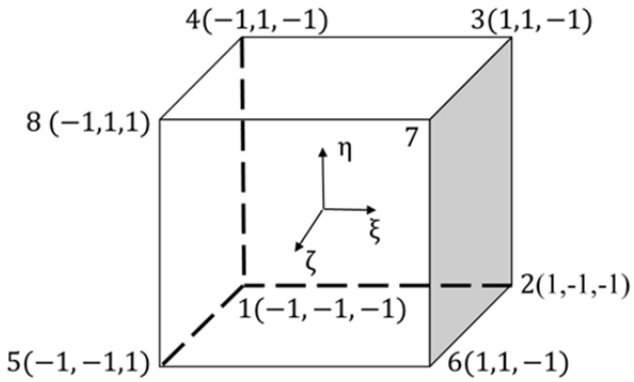

Figure 1. Isoparametric hexahedral element with node number

The stiffness matrix is calculated over each element domain Ω_e using Gauss Quadrature in the usual manner as

$$\mathbf{k_e}(\theta_e) = \iiint_{\Omega_e} \mathbf{B}^T\mathbf{C}'(\theta_e)\mathbf{B}d\Omega \approx \sum_{i=1}^{n_{gp}}\sum_{j=1}^{n_{gp}}\sum_{k=1}^{n_{gp}} \left(W_i W_j W_k \mathbf{B}(\xi_i,\eta_j,\zeta_k)^T \mathbf{C}'(\theta_e)\mathbf{B}(\xi_i,\eta_j,\zeta_k)|\mathbf{J}(\xi_i,\eta_j,\zeta_k)|\right) \quad (3)$$

where n_{gp} is the number of Gauss point in each coordinate direction. The matrix $\mathbf{B}$ is the strain-displacement matrix and $\mathbf{J}$ is the Jacobian matrix, both derived from the shape functions that define the isoparametric mapping in the element. The rotated constitutive matrix $\mathbf{C}'(\theta_e)$ in Equation (3) depends on the non-isotropic material orientation angle θ_e, which is computed from the non-rotated constitutive matrix $\mathbf{C}$ [40] as

$$\mathbf{C}'(\theta_e) = \mathbf{T}(\theta_e)^{-1}\mathbf{C}\mathbf{T}(\theta_e)^{-T} \quad (4)$$

In our simulations, the plane formed by axes ξ and η in Figure 1 is defined as the print plane, such that the orientation variable θ_e rotates about the ζ axis for all elements. Given this constraint on orientation, the inverse of the transformation matrix $\mathbf{T}(\theta)$ becomes

$$\mathbf{T^{-1}}(\theta_e) = \begin{bmatrix} \cos(\theta)^2 & \sin(\theta)^2 & 0 & 0 & 0 & -2\sin(\theta)\cos(\theta) \\ \sin(\theta)^2 & \cos(\theta)^2 & 0 & 0 & 0 & 2\sin(\theta)\cos(\theta) \\ 0 & 0 & 1 & 0 & 0 & 0 \\ 0 & 0 & 0 & \cos(\theta) & \sin(\theta) & 0 \\ 0 & 0 & 0 & -\sin(\theta) & \cos(\theta) & 0 \\ \cos(\theta)\sin(\theta) & -\cos(\theta)\sin(\theta) & 0 & 0 & 0 & \cos(\theta)^2 - \sin(\theta)^2 \end{bmatrix} \tag{5}$$

In the FFF process, suspended carbon fibers become highly aligned with the polymer bead along the print direction, making it feasible to model the material as a transversely isotropic constitutive material described by the matrix $\mathbf{C}$ is written as [41]

$$\mathbf{C} = \begin{bmatrix} \frac{1}{E_x} & -\frac{v_{xy}}{E_x} & -\frac{v_{xy}}{E_x} & 0 & 0 & 0 \\ -\frac{v_{xy}}{E_x} & \frac{1}{E_y} & -\frac{v_{yz}}{E_y} & 0 & 0 & 0 \\ -\frac{v_{xy}}{E_x} & -\frac{v_{yz}}{E_y} & \frac{1}{E_y} & 0 & 0 & 0 \\ 0 & 0 & 0 & \frac{2(1+v_{yz})}{E_y} & 0 & 0 \\ 0 & 0 & 0 & 0 & \frac{1}{G_{xy}} & 0 \\ 0 & 0 & 0 & 0 & 0 & \frac{1}{G_{xy}} \end{bmatrix}^{-1} \tag{6}$$

where material constants are defined in the usual manner and we assume the xyz-axes align with the ξηζ-axes.

Material constants for our simulation appearing in Equation (6) are taken from Heller, et al. [42]. They investigated die-swell in the extruded polymer and its effect on fiber orientation. Furthermore, based on the fiber orientation state, they calculate elastic properties of the extruded polymer composite. The elastic properties of the polymer composites obtained within the extrudate swell region in Heller, et al. (cf. Table 1) are used to define the matrix $\mathbf{C}$ in our analyses. The calculation is based on 15% fiber volume, with $E_f = 240\text{GPa}$, $v_f = 0.2$, $E_m = 2\text{GPa}$ and $v_m = 0.4$. The aspect ratio of the fiber is 15.

E_x	E_y	G_{xy}	v_{xy}	v_{yz}
7.34	3.43	1.39	0.42	0.47

Table 1. Five elastic constants derived from Heller et, al [42], units in Pa

From Table 1, the greater magnitude of E_x than E_y creates a material that lacks isotropy where the E_x is the stiffness along the fiber axis, and E_y is the transverse stiffness of the fiber.

Design Sensitivities

Design sensitivity of the objective function in Equation (1) is derived using the Adjoint Variable Method due to the large numbers of design variables present in the topology optimization problem, i.e., each element has two design variables. For the elemental density design variables, the design sensitivity of compliance is

$$\frac{\partial c}{\partial \rho_e} = -p(\rho_e)^{p-1}\mathbf{u_e^T k_e u_e} \tag{7}$$

Furthermore, the design sensitivity of compliance with respect to an orientation variable is

$$\frac{\partial c}{\partial \theta_e} = \rho_e^p \mathbf{u_e^T}\left\{\iiint_{\Omega_e} \mathbf{B}^T\left(\frac{\partial \mathbf{T}(\theta_e)^{-1}}{\partial \theta_e}\mathbf{C}T(\theta_e)^{-T} + \mathbf{T}(\theta_e)^{-1}\mathbf{C}\frac{\partial \mathbf{T}(\theta_e)^{-T}}{\partial \theta_e}\right)\mathbf{B}d\Omega\right\}\mathbf{u_e} \tag{8}$$

The integrals in the sensitivity expressions in Equations (7) and (8) are calculated with the finite element method using the same Gauss Quadrature as that used in the underling finite element formulation. During the optimization process, a checkerboard pattern is likely to occur, resulting in undesirable structure pattern. To mitigate such effect, a linear sensitivity filter with respect to the density variable [34,35] is employed where the filtered sensitivity becomes

$$\frac{\widehat{\partial c}}{\partial \rho_\imath} = \frac{\sum_{j=1}^{Ne} H_{ij}\,\rho_j \frac{\partial c}{\partial \rho_j}}{\rho_i \sum_{j=1}^{Ne} H_{ij}} \tag{9}$$

with

$$H_{ij} = r_{min} - dist(i,j) \tag{10}$$

In the above, H_{ij} is a weight factor and is a linear function of the distance between the center of element i to the center of neighboring element j.

Optimization Process

Figure 2 shows the flow of the optimization iteration process employed in this work for CFAO of FFF composites. First, the design domain and boundary conditions are defined, and the domain is discretized into hexahedral elements. Second, the FEA model is solved to calculate the global displacement vector; 2-point Gauss Quadrature is used for all element integrations. Third, the compliance objective function and design sensitivities are evaluated element-by-element. Fourth, the design sensitivities with respect to the density variables are filtered using a linear weight average function. Fifth, the objective function and design sensitivities are provided to the Matlab (The Mathworks, Inc, Natick, MA) optimization function *fmincon* [43]. The default solver *interior-point* algorithm is chosen as the optimization scheme which solves the constrained nonlinear problem by introducing extra barrier functions into the objective function. The optimization convergence criteria is based on relative changes in design variables and objective values between two iterations, halting computations when these values are below 0.1%.

In our simulations, the penalty parameter p is chosen to be 3 as is common in topology optimizations, the filter radius r_{min} involved in Equation (10) is set to be 1.5, the volume fraction limit f = 0.4, and the density variables are allowed to range from 10^{-6} to 1.

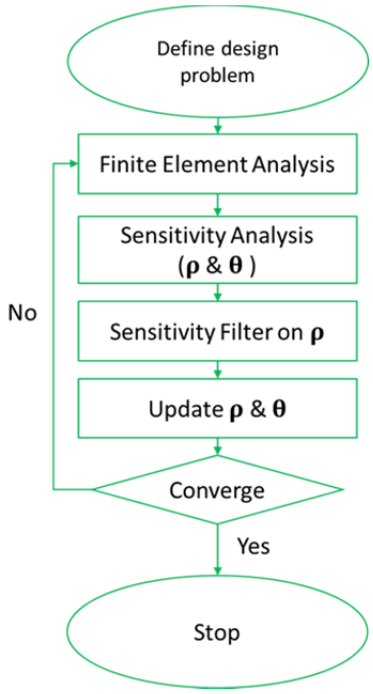

Figure 2. Flow chart demonstrating the process of topology optimization

Once convergence of the optimization is achieved, the elements that have density value greater than 0.5 are plotted to illustrate the optimized topology; the darker the element, the more material is assigned to the element, and vice versa. The corresponding fibers (red segments) are also plotted inside each 3D finite element to show the direction of preferred material orientation. Also, in viewing the angle that is orthogonal to the print plane, the layer-by-layer plots are shown to illustrate the details of the material distribution and material orientation in each layer. Lastly, the computational time, the number of iterations and the computed compliance are recorded. It is important to note that all the code for optimization were developed in-house, except the *fmincon* optimization algorithm.

Numerical Examples

A cantilever beam with a unit point load on center of the right bottom edge is considered for the optimization as shown in Figure 3. To investigate how the print direction affects the optimized topology and minimized compliance, the optimization is performed in each of the three coordinate directions. Considering Figure 3, the x-y plane defines the print plane, and the simulated model is assumed to be printed as follows:

- Case 1: Printed from the back face to the front face with 20x10x6 elements
- Case 2: Printed from the bottom face to the top face with 20x6x10 elements
- Case 3: Printed from the left face to the right face with 10x6x20 elements

The topology design optimization problem included a total of 2400 design variable in each of these print cases, 1200 ρ_e and 1200 θ_e. In all cases, elements are formed as cubes having sides of 1 unit in length.

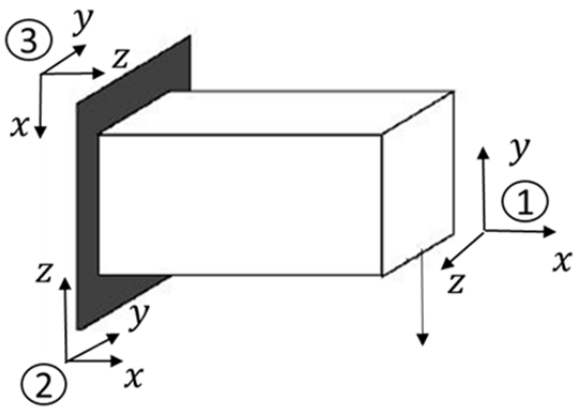

Figure 3. Cantilever beam with tip point load

Computational results

Figure 4 shows the optimized topologies in isometric views for Case 1, Case 2 and Case 3. Overall, the optimized topologies for all three cases converged to a similar I-beam type structure, where the beam is wide at the top and bottom layers. Regardless of which direction the structure is printed, there is dense material distributed to two wide flanges, which increases the stiffness in support of the bending load.

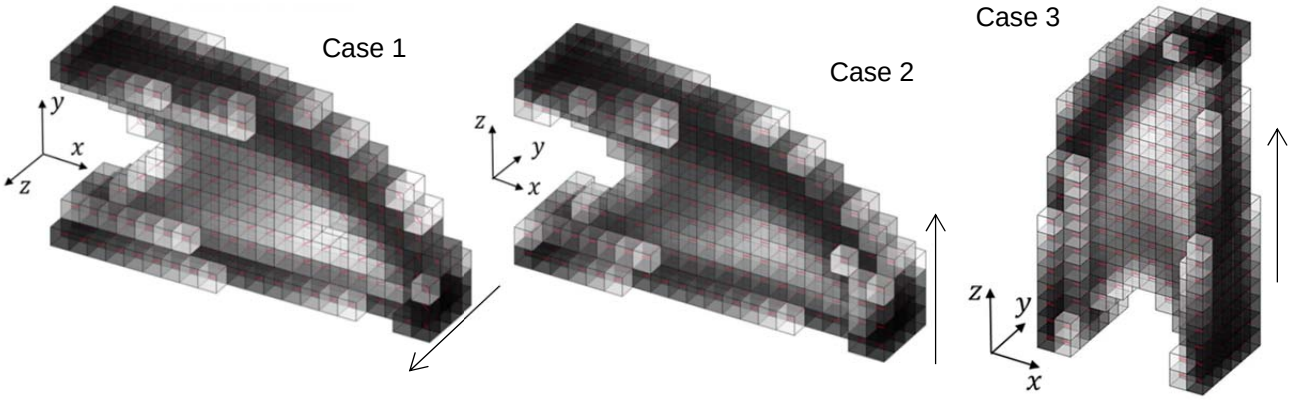

Figure 4. Optimized topologies for three cases (isometric views). Arrows indicate print direction.

Figure 5, Figure 6 and Figure 7 reveal the layer-by-layer plots of the optimized material distribution and material orientation for the three cases, when the viewer is looking at the direction orthogonal to the print plane. Figure 5 shows the layer-by-layer material distribution and material orientation for Case 1. Note that since the load is applied at the center of the right bottom edge (cf. Figure 3), we would expect the optimized structure to exhibit geometric symmetry in terms of both the material distribution and material orientation. By comparing the layout of layer 1 to lay 6, layer 2 to layer 5 and layer 3 to layer 4, the pairs look visually identical, which confirms our hypothesis. In terms of the material orientation, the fibers follow

the outer contour of the structure for each layer where there is dense material distributed, which is very similar to results given by Hoglund and Smith [44] and Nomura, et al. [45].

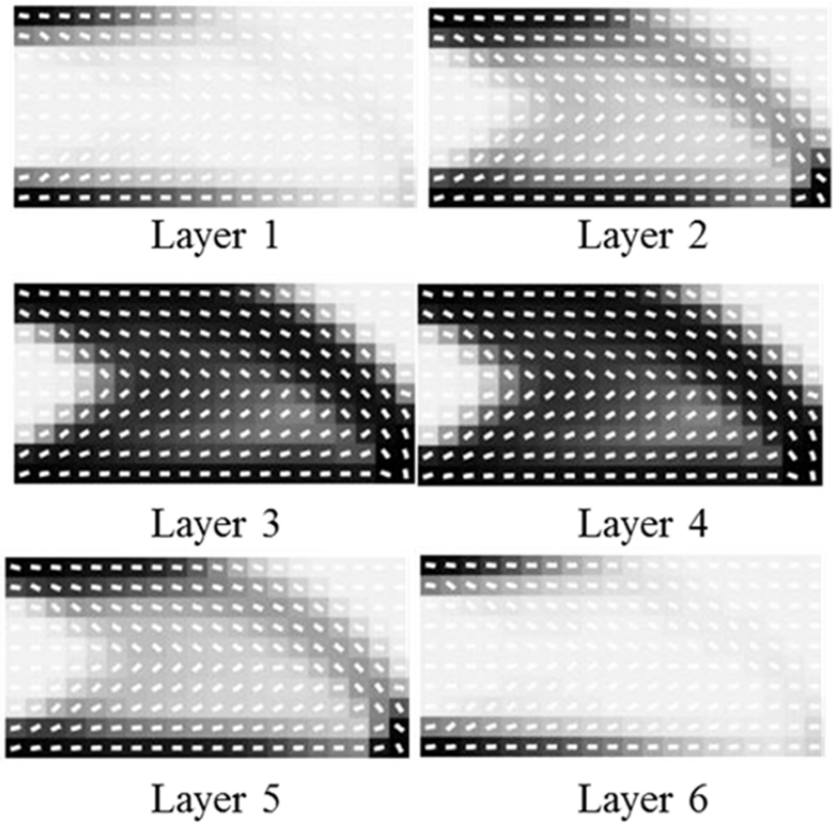

Figure 5. Layer-by-layer plots of material distribution and material orientation for Case 1 (front view).). Layer 1, which corresponds to the layer at the back layer, progresses to layer 6, which corresponds to layer of the front layer.

Figure 6 shows layer-by-layer plots for the material distribution and material orientation for Case 2. Most of the fibers point toward the point of load application, which accommodates the increased material stiffness in the fiber direction. Furthermore, the symmetry of material distribution and material orientation exists in each layer by comparing the first three layers counting form the top to the three layers counting from the bottom.

Figure 7 shows the material distribution and material orientation at each layer for Case 3. The scenario here is very much like the same as that described for Case 2. Visually speaking, there is material distribution and material orientation symmetry in each layer by comparing the first three layers counting form the top to the three layers counting from the bottom.

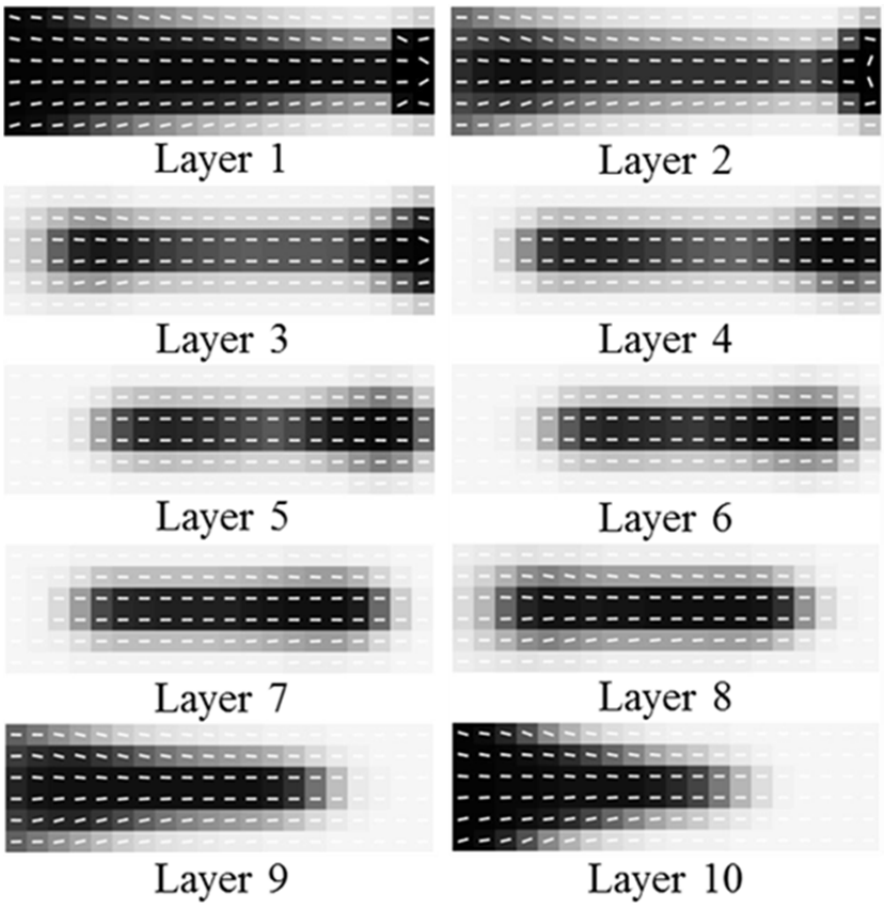

Figure 6. Layer-by-layer plots of material distribution and material orientation for Case 2 (top view). Layer 1, which corresponds to the bottom layer of the optimized structure, moves up toward layer 10, which corresponds to the top layer of the optimized structure.

Table 2 compares the computation CPU time, the number of iterations and the compliance for the three cases. Case 1 took about 48.8% and 70.8% of more CPU time than Case 2 and Case 3 to achieve convergence, as well as 24 and 31 more iterations, respectively. However, Case 1 yields about 23% and 63% lower compliance than Case 2 and Case 3, respectively. Since the orientation rotates in plane with the force in Case 1, the structure's compliance is very sensitive to the material orientation and can therefore be more easily affected by the state of material orientation. However, for Case 2 and Case 3, the plane of rotation does not align with the force direction; therefore the material orientation optimization yields less improvement in terms of the compliance. From this study, one important lesson we can draw is that how effective the FFF print technique is to produce a safe structure depends greatly on whether the designers can correctly anticipating the loading direction.

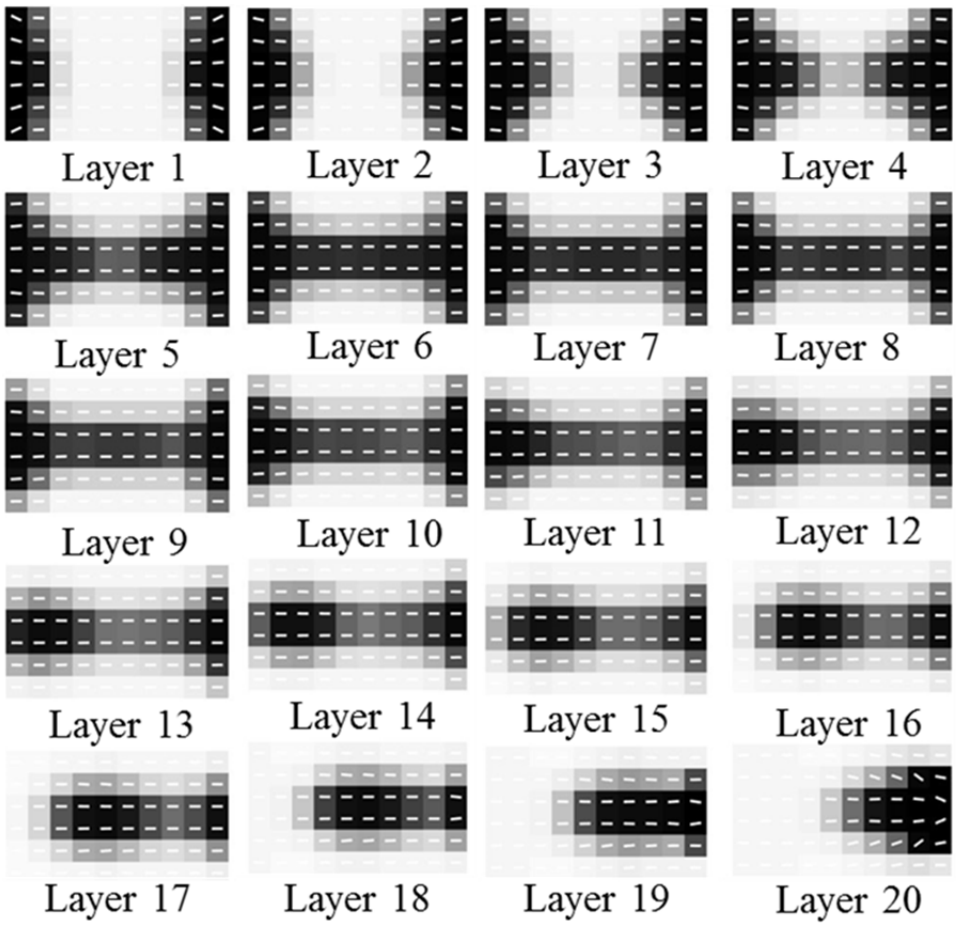

Figure 7. Layer-by-layer plots of material distribution and material orientation for Case 2 (right view). Layer 1 starting from the bottom to layer 20 to the top layer of the optimized structure

	CPU time (sec)	Iterations	Compliance (N*m)
Case 1	246.3	78	3.48
Case 2	165.5	54	4.28
Case 3	144.2	47	5.66

Table 2. Topology result comparisons among three cases, for computational time, number of iterations and compliance

Conclusions

In conclusion, we have extended the SIMP with CFAO and implemented it using the Matlab *fmincon* optimization function to solve 3D topology optimization problems for FFF. The optimization objective is the compliance of structure that is minimized in the computations. The objective and constraints, and design sensitivities are calculated using Finite Element Analysis with linear eight node isoparametric element. Design sensitivity expressions are derived using the Adjoint Variable method which reduces to an element level evaluation. Furthermore, a linear weighted sensitivity filter is employed to mitigate checkerboarding of the material distribution. A 3D cantilever beam was optimized where we considered 3 different print directions. For the

problem we studied in printing at multiple planes, the designs where material rotation plane aligns with the force direction gives the lowest compliance. Furthermore, printing the structure at different plane direction does affect the compliance result, which is important for designers to consider when designing 3D printed parts with non-isotropic material microstructures.

References

[1] Sung-Hoon Ahn, Michael Montero, Dan Odell, Shad Roundy, and Paul K. Wright, 2002, "Anisotropic Material Properties of Fused Deposition Modeling ABS," Rapid Prototyp. J., **8**(4), pp. 248–257.

[2] Ziemian, C., Sharma, M., and Ziemi, S., 2012, "Anisotropic Mechanical Properties of ABS Parts Fabricated by Fused Deposition Modelling," *Mechanical Engineering*, M. Gokcek, ed., InTech.

[3] Bagsik, A. and Schöppner, V., 2011, "Mechanical Properteis of Fused Deposition Modeling Parts Manufactured with Ultem*9085," ANTEC 2011, Boston, MA.

[4] Wohlers, T., 2016, *Wohlers Report 2016*, Wohlers Associates, Inc.

[5] Perez, A. R. T., Roberson, D. A., and Wicker, R. B., 2014, "Fracture Surface Analysis of 3D-Printed Tensile Specimens of Novel ABS-Based Materials," J. Fail. Anal. Prev., **14**(3), pp. 343–353.

[6] Zhong, W., Li, F., Zhang, Z., Song, L., and Li, Z., 2001, "Short Fiber Reinforced Composites for Fused Deposition Modeling," Mater. Sci. Eng. A, **301**(2), pp. 125–130.

[7] Gray, R. W., Baird, D. G., and Bøhn, J. H., 1998, "Thermoplastic Composites Reinforced with Long Fiber Thermotropic Liquid Crystalline Polymers for Fused Deposition Modeling," Polym. Compos., **19**(4), pp. 383–394.

[8] Shofner, M. L., Lozano, K., Rodríguez-Macías, F. J., and Barrera, E. V., 2003, "Nanofiber-Reinforced Polymers Prepared by Fused Deposition Modeling," J. Appl. Polym. Sci., **89**(11), pp. 3081–3090.

[9] Hwang, S., Reyes, E. I., Moon, K., Rumpf, R. C., and Kim, N. S., 2014, "Thermo-Mechanical Characterization of Metal/Polymer Composite Filaments and Printing Parameter Study for Fused Deposition Modeling in the 3D Printing Process," J. Electron. Mater., **44**(3), pp. 771–777.

[10] Dul, S., Fambri, L., and Pegoretti, A., 2016, "Fused Deposition Modelling with ABS–graphene Nanocomposites," Compos. Part Appl. Sci. Manuf., **85**, pp. 181–191.

[11] Ning, F., Cong, W., Qiu, J., Wei, J., and Wang, S., 2015, "Additive Manufacturing of Carbon Fiber Reinforced Thermoplastic Composites Using Fused Deposition Modeling," Compos. Part B Eng., **80**, pp. 369–378.

[12] Tekinalp, H. L., Kunc, V., Velez-Garcia, G. M., Duty, C. E., Love, L. J., Naskar, A. K., Blue, C. A., and Ozcan, S., 2014, "Highly Oriented Carbon Fiber–polymer Composites via Additive Manufacturing," Compos. Sci. Technol., **105**, pp. 144–150.

[13] Jiang, D. and Smith, D. E., 2017, "Mechanical Behavior of Carbon Fiber Composites Produced with Fused Filament Fabrication," In press, Additive Manufacturing.

[14] Love, L. J., Kunc, V., Rios, O., Duty, C. E., Elliott, A. M., Post, B. K., Smith, R. J., and Blue, C. A., 2014, "The Importance of Carbon Fiber to Polymer Additive Manufacturing," J. Mater. Res., **29**(17), pp. 1893–1898.

[15] Post, B., Lloyd, P. D., Lindahl, J., Lind, R. F., Love, L. J., and Kunc, V., 2016, *The Economics of Big Area Addtive Manufacturing*, Oak Ridge National Laboratory (ORNL),

Oak Ridge, TN (United States). Manufacturing Demonstration Facility (MDF), web.ornl.gov/sci/manufacturing/
[16] Spinnie, N. K. , 2016, "Large Scale Fused Deposition Modeling : The Effect of Process Parameters on Bead Geometry.," Master's Thesis, Baylor University.
[17] Suzuki, K., and Kikuchi, N., 1991, "A Homogenization Method for Shape and Topology Optimization," Comput. Methods Appl. Mech. Eng., **93**(3), pp. 291–318.
[18] Bendsøe, M. P., and Kikuchi, N., 1988, "Generating Optimal Topologies in Structural Design Using a Homogenization Method," Comput. Methods Appl. Mech. Eng., **71**(2), pp. 197–224.
[19] Bendsøe, M. P., 1989, "Optimal Shape Design as a Material Distribution Problem," Struct. Optim., **1**(4), pp. 193–202.
[20] Mlejnek, H. P., 1992, "Some Aspects of the Genesis of Structures," Struct. Optim., **5**(1–2), pp. 64–69.
[21] Zhou, M., and Rozvany, G. I. N., 1991, "The COC Algorithm, Part II: Topological, Geometrical and Generalized Shape Optimization," Comput. Methods Appl. Mech. Eng., **89**(1–3), pp. 309–336.
[22] Sigmund, O., 2001, "A 99 Line Topology Optimization Code Written in Matlab," Struct. Multidiscip. Optim., **21**(2), pp. 120–127.
[23] Andreassen, E., Clausen, A., Schevenels, M., Lazarov, B. S., and Sigmund, O., 2011, "Efficient Topology Optimization in MATLAB Using 88 Lines of Code," Struct. Multidiscip. Optim., **43**(1), pp. 1–16.
[24] Liu, K., and Tovar, A., 2014, "An Efficient 3D Topology Optimization Code Written in Matlab," Struct. Multidiscip. Optim., **50**(6), pp. 1175–1196.
[25] Xie, Y. M., and Steven, G. P., 1993, "A Simple Evolutionary Procedure for Structural Optimization," Comput. Struct., **49**(5), pp. 885–896.
[26] Tang, Y., Kurtz, A., and Zhao, Y. F., 2015, "Bidirectional Evolutionary Structural Optimization (BESO) Based Design Method for Lattice Structure to Be Fabricated by Additive Manufacturing," Comput.-Aided Des., **69**, pp. 91–101.
[27] Zhang, P., Toman, J., Yu, Y., Biyikli, E., Kirca, M., Chmielus, M., and To, A. C., 2015, "Efficient Design-Optimization of Variable-Density Hexagonal Cellular Structure by Additive Manufacturing: Theory and Validation," J. Manuf. Sci. Eng., **137**(2), pp. 021004-021004-8.
[28] Gaynor, A. T., Meisel, N. A., Williams, C. B., and Guest, J. K., 2014, "Multiple-Material Topology Optimization of Compliant Mechanisms Created Via PolyJet Three-Dimensional Printing," J. Manuf. Sci. Eng., **136**(6), pp. 061015-061015-10.
[29] Langelaar, M., 2016, "Topology Optimization of 3D Self-Supporting Structures for Additive Manufacturing," Addit. Manuf., **12**, Part A, pp. 60–70.
[30] Jia, H. P., Jiang, C. D., Li, G. P., Mu, R. Q., Liu, B., and Jiang, C. B., 2008, "Topology Optimization of Orthotropic Material Structure," Mater. Sci. Forum, **575–578**, pp. 978–989.
[31] Hoglund, R., and Smith, D. E., 2015, "Non-Isotropic Material Distribution Topology Optimization for Fused Deposition Modeling Products," Proceeding of the 2015 Solid Freeform Fabrication Symposium, Austin, TX.
[32] Bruyneel, M., and Fleury, C., 2002, "Composite Structures Optimization Using Sequential Convex Programming," Adv. Eng. Softw., **33**(7–10), pp. 697–711.

[33] Lindgaard, E., and Lund, E., 2011, "Optimization Formulations for the Maximum Nonlinear Buckling Load of Composite Structures," Struct. Multidiscip. Optim., **43**(5), pp. 631–646.
[34] Sigmund, O., and Petersson, J., 1998, "Numerical Instabilities in Topology Optimization: A Survey on Procedures Dealing with Checkerboards, Mesh-Dependencies and Local Minima," Struct. Optim., **16**(1), pp. 68–75.
[35] Sigmund, O., 2007, "Morphology-Based Black and White Filters for Topology Optimization," Struct. Multidiscip. Optim., **33**(4–5), pp. 401–424.
[36] Setoodeh, S., Abdalla, M. M., and Gürdal, Z., 2005, "Combined Topology and Fiber Path Design of Composite Layers Using Cellular Automata," Struct. Multidiscip. Optim., **30**(6), pp. 413–421.
[37] Nomura, T., Dede, E. M., Lee, J., Yamasaki, S., Matsumori, T., Kawamoto, A., and Kikuchi, N., 2015, "General Topology Optimization Method with Continuous and Discrete Orientation Design Using Isoparametric Projection," Int. J. Numer. Methods Eng., **101**(8), pp. 571–605.
[38] Hoglund, R. M., 2016, "An Anisotropic Topology Optimization Method for Carbon Fiber-Reinforced Fused Filament Fabrication.," Master's Thesis, Baylor University.
[39] Reddy, J., 2005, *An Introduction to the Finite Element Method*, McGraw-Hill Education.
[40] Barbero, E. J., 2010, *Introduction to Composite Materials Design, Second Edition*, CRC Press.
[41] Kollár, L. P., and Springer, G. S., 2003, *Mechanics of Composite Structures*, Cambridge University Press.
[42] Heller, B. P., Smith, D. E., and Jack, D. A., 2016, "Effects of Extrudate Swell and Nozzle Geometry on Fiber Orientation in Fused Filament Fabrication Nozzle Flow," Addit. Manuf., **12**, Part B, pp. 252–264.
[43] "Find Minimum of Constrained Nonlinear Multivariable Function - MATLAB Fmincon" [Online]. Available: https://www.mathworks.com/help/optim/ug/fmincon.html. [Accessed: 17-Dec-2016].
[44] Hoglund, R., and Smith, D. E., 2016, "Continuous Fiber Angle Topology Optimizatin for Polymer Fused Filament Fabrication," Proceedings of the 2016 Solid Freeform Fabrication Symposium, Austin, TX.
[45] Nomura, T., Dede, E. M., Lee, J., Yamasaki, S., Matsumori, T., Kawamoto, A., and Kikuchi, N., 2015, "General Topology Optimization Method with Continuous and Discrete Orientation Design Using Isoparametric Projection," Int. J. Numer. Methods Eng., **101**(8), pp. 571–605.